Articles

Synthesis and Properties of Monoclinic and Cubic Forms of the A-Site-Ordered $(BiMn_3)Mn_4O_{12}$ Perovskite

Naoki Imamura,[†] Maarit Karppinen,*[,†,‡] and Hisao Yamauchi[†,‡]

Materials and Structures Laboratory, Tokyo Institute of Technology, Yokohama 226-8503, Japan, and Laboratory of Inorganic Chemistry, Department of Chemistry, Helsinki University of Technology, FI-02015 TKK, Finland

Received November 7, 2008. Revised Manuscript Received April 4, 2009

We have obtained two new A-site-ordered manganese perovskite oxides with the common chemical formula of $(BiMn_3)Mn_4O_{12\pm\delta}$ with regard to their metal composition. The two phases were prepared through high-pressure synthesis under identical conditions except for the oxygen-to-metal ratio in the precursor mixture. Accordingly, they were found to differ from each other in the oxygen content. The less-oxidized phase possesses a monoclinic crystal structure and shows two magnetic transitions, at 28 and 59 K, whereas the more-strongly-oxidized and hence denser phase with a cubic crystal structure lacks the higher-temperature transition. Thus, the present work has demonstrated an attractive but not-yet-utilized possibility to tailor the properties of $(A'A''_3)B_4O_{12\pm\delta}$-type cation-ordered perovskite oxides by means of oxygen-content control.

Perovskite manganese oxides have attracted considerable attention due to their amazing functional properties, such as their colossal magnetoresistance[1] and multiferroic[2] effects. In these oxide materials, a tiny change in the crystal structure and/or the valence state of manganese—sensitively tuned by means of chemical substitution and/or oxygen-content control—may trigger a magnified change in the desired functional properties. In recent years, the interest has expanded from the simple $AMnO_3$ perovskites to various cation-ordered perovskite phases, such as $A_2(MnB'')O_6$,[3−5] $(A'A'')Mn_2O_6$,[6−9] and $(A'A''_3)Mn_4O_{12}$,[10−14] in which one of the cation sites is occupied by two different cation species. The present work is focused on the last of these three systems. In the $(A'A''_3)Mn_4O_{12}$ system, the two different A-site cations, A′ and A″, are ordered in a one-to-three arrangement. Here it is interesting to note that simultaneously A- and B-site-ordered $(A'A''_3)(B'_2B''_2)O_{12}$-type phases have been reported as well (but not for B′ = Mn), i.e., $(CaCu_3)(B'_2B''_2)O_{12}$ with B′ = Ga or Cr and B″ = Ru, Sb, or Ta.[15]

Stabilization of the $(A'A''_3)Mn_4O_{12}$ structure requires that the A″-site is occupied by a Jahn-Teller (JT) active species, i.e., divalent copper or trivalent manganese. The choice of A″ has a strong influence on the properties of the phase: compounds with Cu^{2+} at the A″-site are electrically conductive, whereas those with Mn^{3+} at the A″-site are insulators.[11−14] Besides the cation composition, properties of complex transition metal oxides are traditionally adjusted through oxygen-content control. As for the $(A'A''_3)B_4O_{12}$ perovskites, efforts to control the oxygen content have been rare. In fact, little is known about the oxygen content and its tunability in the $(A'A''_3)B_4O_{12}$ system. One reason is that most of the $(A'A''_3)B_4O_{12}$ compounds are insoluble in diluted acidic solutions; hence, redox titration techniques, conventionally employed for the precise oxygen-

* To whom correspondence should be addressed. E-mail: maarit.karppinen@tkk.fi.
† Tokyo Institute of Technology.
‡ Helsinki University of Technology.

(1) Tokura, Y.; Urushibara, A.; Moritomo, Y.; Arima, T.; Asamitsu, A.; Kido, G.; Furukawa, N. *J. Phys. Soc. Jpn.* **1994**, *63*, 3931.
(2) Kimura, T.; Goto, T.; Shintani, H.; Ishizaka, K.; Arima, T.; Tokura, Y. *Nature (London)* **2003**, *426*, 55.
(3) Dass, R. I.; Yan, J.-Q.; Goodenough, J. B. *Phys. Rev. B* **2003**, *68*, 064415.
(4) Rogado, N. S.; Li, J.; Sleight, A. W.; Subramanian, M. A. *Adv. Mater.* **2005**, *17*, 2225.
(5) Azuma, M.; Takata, K.; Saito, T.; Ishiwata, S.; Shimakawa, Y.; Takano, M. *J. Am. Chem. Soc.* **2005**, *127*, 8889.
(6) Chapman, J. P.; Attfield, J. P.; Molgg, M.; Friend, C. M.; Beales, T. P. *Angew. Chem., Int. Ed. Engl.* **1996**, *35*, 2482.
(7) Caignaert, V.; Millange, F.; Domengès, B.; Raveau, B.; Suard, E. *Chem. Mater.* **1999**, *11*, 930.
(8) Nakajima, T.; Kageyama, H.; Yoshizawa, H.; Ueda, Y. *J. Phys. Soc. Jpn.* **2002**, *71*, 2843.
(9) Karppinen, M.; Okamoto, H.; Fjellvåg, H.; Motohashi, T.; Yamauchi, H. *J. Solid State Chem.* **2004**, *177*, 2122.
(10) Bochu, B.; Chenavas, J.; Joubert, J. C.; Marezio, M. *J. Solid State Chem.* **1974**, *11*, 88.
(11) Zeng, Z.; Greenblatt, M.; Subramanian, M. A.; Croft, M. *Phys. Rev. Lett.* **1999**, *82*, 3164.
(12) Prodi, A.; Gilioli, E.; Gauzzi, A.; Licci, F.; Marezio, M.; Bolzoni, F.; Huang, Q.; Santoro, A.; Lynn, J. W. *Nat. Mater.* **2004**, *3*, 48.
(13) Takata, K.; Yamada, I.; Azuma, M.; Takano, M.; Shimakawa, Y. *Phys. Rev. B* **2007**, *76*, 024429.
(14) Imamura, N.; Karppinen, M.; Motohashi, T.; Fu, D.; Itoh, M.; Yamauchi, H. *J. Am. Chem. Soc.* **2008**, *130*, 14948.
(15) Byeon, S.-H.; Lufaso, M. W.; Parise, J. B.; Woodward, P. M.; Hansen, T. *Chem. Mater.* **2003**, *15*, 3798. Byeon, S.-H.; Lee, S.-S.; Parise, J. B.; Woodward, P. M.; Hur, N. H. *Chem. Mater.* **2004**, *16*, 3697. Byeon, S.-H.; Lee, S.-S.; Parise, J. B.; Woodward, P. M.; Hur, N. H. *Chem. Mater.* **2005**, *17*, 3552. Byeon, S.-H.; Lee, S.-S.; Parise, J. B.; Woodward, P. M. *Chem. Mater.* **2006**, *18*, 3873.

10.1021/cm803030x CCC: $40.75
Published on Web 05/04/2009

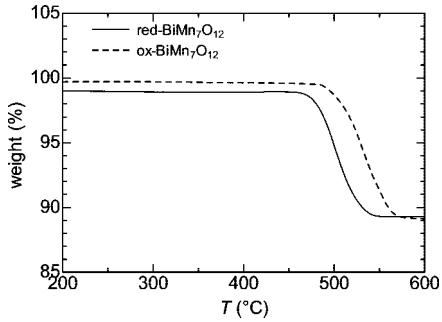

Figure 1. Representative TG-reduction curves for samples obtained through the two different synthesis routes, route 1 (red-$BiMn_7O_{12}$) and route 2 (ox-$BiMn_7O_{12}$).

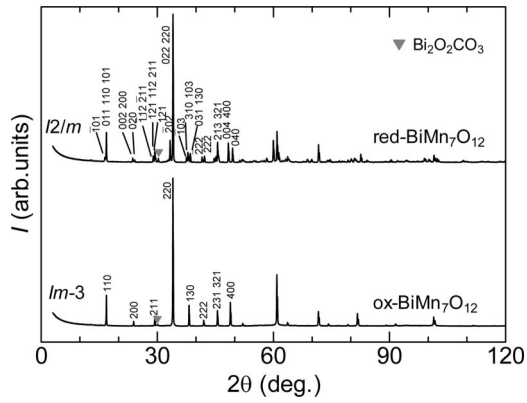

Figure 2. XRD patterns for the two new phases, red-$BiMn_7O_{12}$ and ox-$BiMn_7O_{12}$.

content analysis of perovskite oxides, cannot be used here for the task. Another reason is that the $(A'A''_3)B_4O_{12}$ compounds are prone to cation-mixing between the A″ and B cations,[16,17] which makes the compositional analysis difficult.

In the $(A'Mn_3)Mn_4O_{12}$-type compound with a trivalent A′-site constituent, the A″- and B-sites are both occupied by trivalent manganese, and accordingly, the A″/B cation-mixing effect does not play any role. Such perovskites (with A′ = La, Nd) were realized through high-pressure synthesis already in 1974.[10] However, no attention was paid to the oxygen content. Here we demonstrate for our recently discovered $(BiMn_3)Mn_4O_{12\pm\delta}$ system[14] that just like for a majority of perovskite oxides the oxygen content is controllable for the $(A'A''_3)B_4O_{12}$-type perovskites as well. Moreover, it is shown that both the crystal structure and the magnetic properties are highly sensitive to the oxygen content/valence state of manganese in $(BiMn_3)Mn_4O_{12\pm\delta}$. Here it should be emphasized that the $(BiMn_3)Mn_4O_{12\pm\delta}$ system, in which the A′-cation site is occupied by trivalent bismuth instead of a trivalent rare earth element, is highly interesting, as it was revealed to exhibit exciting magnetodielectric properties.[14]

Polycrystalline samples of $(BiMn_3)Mn_4O_{12\pm\delta}$ or $BiMn_7O_{12\pm\delta}$ were prepared by means of high-pressure (HP) synthesis[14] using stoichiometric (in terms of metal composition) mixtures of Bi_2O_3 and Mn_2O_3 as raw materials. The

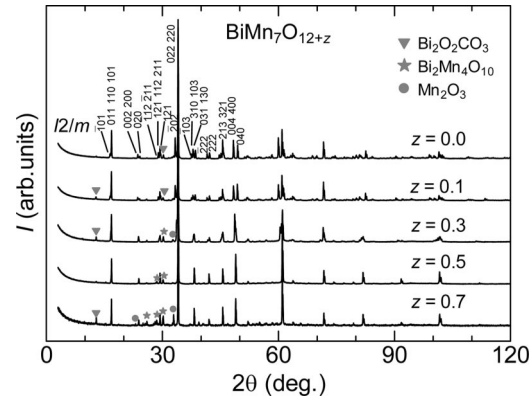

Figure 3. XRD patterns for the $BiMn_7O_{12+z}$ samples synthesized with different $Mn_2O_3/2MnO_2$ ratios in the raw material mixture and accordingly different nominal oxygen contents, z.

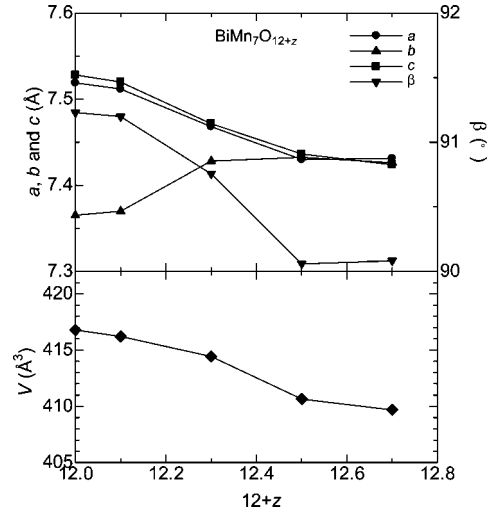

Figure 4. Lattice parameters, a (●), b (▲), c (■), and β (▼), and the unit-cell volume, V (◆), for the $BiMn_7O_{12+z}$ samples plotted in terms of the nominal oxygen content, $12 + z$.

Bi_2O_3 powder was calcined *prior* to use in air at 300 °C, whereas the Mn_2O_3 powder was freshly synthesized for each sample batch from $MnCO_3$ through firing in air at 850 °C. The following two different synthesis routes were employed: in route 1, the raw material powder mixture (Bi_2O_3 + $7Mn_2O_3$) was loaded without any pretreatment in a gold capsule for the HP synthesis, whereas in route 2, the raw material mixture was first heated in air at 600 °C for 8 h to obtain a precursor consisting of two ternary oxide phases of $Bi_2Mn_4O_{10}$ and $Bi_{12}MnO_{20}$ as well as the raw binary oxides Bi_2O_3 and Mn_2O_3. Note that both the ternary oxides are more highly oxidized than the binary oxides and hence the precursor prepared through route 2 acts as a kind of "internal oxygen source" in the HP synthesis. Additionally, a sample series was synthesized (without the preheating step in air) in which a part of Mn_2O_3 in the raw material mixture was replaced by $2MnO_2$. Here the purpose was to gradually increase the excess oxygen content in the raw material mixture. For all the samples, the final HP synthesis was carried out under identical conditions in a cubic-anvil-type HP apparatus at 5 GPa and 1100 °C for 30 min.

The metal composition of the samples was determined by ICP-AES (inductively coupled plasma atomic emission spectrometer; Shimadzu ICPS-8100) analysis. The two synthesis

(16) Avdeev, M.; Nalbandyan, V. B. *Inorg. Chem.* **2006**, *45*, 2217.
(17) Presniakov, I. A.; Rusakov, V. S.; Gubaidulina, T. V.; Sobolev, A. V.; Baranov, A. V.; Demazeau, G.; Volkova, O. S.; Cherepanov, V. M.; Goodilin, E. A.; Knot'ko, A. V.; Isobe, M. *Phys. Rev. B* **2007**, *76*, 214407.

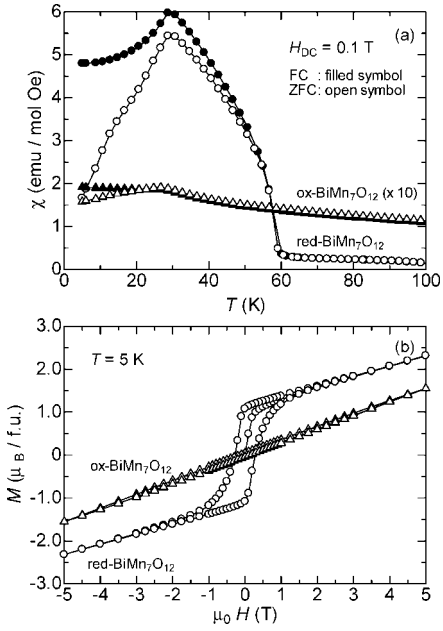

Figure 5. Magnetic properties of red-$BiMn_7O_{12}$ and ox-$BiMn_7O_{12}$: (a) temperature dependence of dc magnetic susceptibility χ measured under an external magnetic field of 0.1 T in both FC and ZFC modes and (b) magnetic field dependence of magnetization, M. The $M-H$ curves were recorded at 5 K.

routes were both confirmed—within the precision (95%) of the analysis method—to yield samples with an essentially nominal Bi:Mn molar ratio, i.e., 0.97:7 for route 1 and 0.96:7 for route 2. Then the oxygen-to-metal ratio of the samples was determined by thermogravimetric (TG) reduction experiments carried out in 5% H_2/Ar gas flow[18] up to 600 °C in a thermobalance of high sensitivity (Mac Science: TG-DTA 2000S). In these TG runs the sample mass was ~10 mg and the heating rate was 1 °C/min. Figure 1 displays representative TG curves obtained for the two types of the sample. From Figure 1, the $BiMn_7O_{12\pm\delta}$ samples are (independent of the type) found to decompose around 500 °C to a mixture of Bi and MnO (as confirmed by XRD; not shown here) according to a single-step reduction reaction: $Bi_xMn_yO_z \rightarrow x\mathrm{Bi} + y\mathrm{MnO} + 0.5(z-y)O_2$. Since the ratio x:y is known from the ICP-AES analysis, the amount of oxygen (with respect to the total metal content, $x + y$) could be calculated from the TG data in a straightforward manner. It was revealed that the samples synthesized through route 2 are more strongly oxidized than those obtained through route 1. Expressing the results such that the Mn content is set at 7, our combined ICP-AES and TG analysis yielded, as the sample stoichiometry, $Bi_{0.97}Mn_{7.00}O_{11.95}$ (route 1) and $Bi_{0.96}Mn_{7.00}O_{12.16}$ (route 2). Note that the given numbers are mean values of several parallel experiments: the ICP-AES analysis was repeated 10 times and the TG analysis seven times for both the sample types, with reproducibility better than ±0.005 for the Bi content and ±0.1 for the oxygen content. It should also be emphasized that the perovskite framework allows rather cation vacancies but no oxygen interstitials. Hence, the composition given above for samples synthesized through route 2 should be rather expressed as $Bi_{0.94}Mn_{6.91}O_{12}$. Hereafter—for the sake of simplicity—we refer to the more reduced samples obtained through route 1 as red-$BiMn_7O_{12}$ and to the more oxidized samples obtained through route 2 as ox-$BiMn_7O_{12}$.

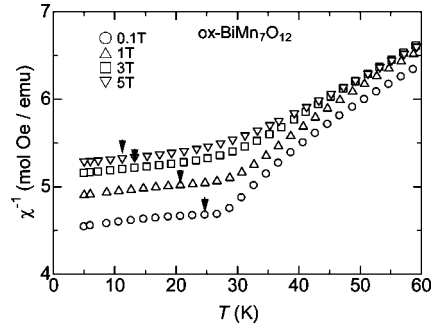

Figure 6. Temperature dependence of inverse FC susceptibility for ox-$BiMn_7O_{12}$ measured under various magnetic fields. The onset of the plateau is represented by the arrows.

The samples were characterized for phase purity and crystal structure by room-temperature X-ray powder diffraction (XRD; Rigaku: RINT2550VK/U equipped with a rotating Cu anode). In Figure 2 are shown representative XRD patterns for our red-$BiMn_7O_{12}$ and ox-$BiMn_7O_{12}$ samples. Both samples were found free from unwanted impurity phases except for a trace of $Bi_2O_2CO_3$. For red-$BiMn_7O_{12}$, the pattern was readily indexed (using JANA2000[19] for profile fitting) in the same monoclinic space group, i.e., $I2/m$, as previously reported for $(LaMn_3)Mn_4O_{12}$ at room temperature,[10] and the lattice parameters were accordingly determined at $a = 7.548(3)$ Å, $b = 7.393(3)$ Å, $c = 7.556(3)$ Å, $\beta = 91.229(2)°$. For ox-$BiMn_7O_{12}$, the pattern was best indexed on the basis of the cubic perovskite structure of space group $Im\bar{3}$ with the lattice parameter $a = 7.448$ Å as previously reported for various high-temperature phases of $(A'Mn_3)Mn_4O_{12}$ perovskites.[12,20,21] From the lattice parameters determined for red-$BiMn_7O_{12}$ and ox-$BiMn_7O_{12}$ samples, the cubic $(BiMn_3)Mn_4O_{12\pm\delta}$ structure is denser (lattice volume per formula unit = 206.6 Å^3) than the monoclinic one (208.4 Å^3), in accordance with its higher oxygen-to-metal ratio.

Now let us pay attention to the sample series in which the nominal oxygen-to-metal ratio was gradually increased by controlling the Mn_2O_3/2 MnO_2 ratio in the raw material mixture. Here we may find further evidence for the dependence of the (room-temperature) structure of $(BiMn_3)Mn_4O_{12\pm\delta}$ on the oxygen content/cation-vacancy concentration in $(BiMn_3)Mn_4O_{12\pm\delta}$. X-ray diffraction patterns for these $BiMn_7O_{12+z}$ samples with $z = 0.0$, 0.1, 0.3, 0.5, and 0.7 are shown in Figure 3. Despite the fact that the sample quality becomes somewhat lower with increasing z (as seen from the appearance of peaks due to impurity phases, Mn_2O_3, $Bi_2O_2CO_3$, and $Bi_2Mn_4O_{10}$ in Figure 3), it is clearly revealed that the crystal symmetry of the $(BiMn_3)Mn_4O_{12\pm\delta}$ perovskite phase gradually changes from monoclinic to cubic as the nominal oxygen content increases. We refined the lattice parameters for all the $BiMn_7O_{12+z}$ samples using the monoclinic space group $I2/m$; the results are shown in Figure 4. With increasing z, gradual suppression of the monoclinic

(18) Karppinen, M.; Niinistö, L.; Yamauchi, H. *J. Therm. Anal. Calorim.* **1997**, *48*, 1123.
(19) Petricek, V.; Dusek, M.; Palatinus, L. Institute of Physics, Praha, Czech Republic, 2000.
(20) Troyanchuk, I. O.; Chobot, A. N. *Crystallogr. Rep.* **1997**, *42*, 983.
(21) Przenisło, R.; Sosnowska, I.; Suard, E.; Hewat, A.; Fitch, A. N. *J. Phys.: Condens. Matter* **2002**, *14*, 5747.

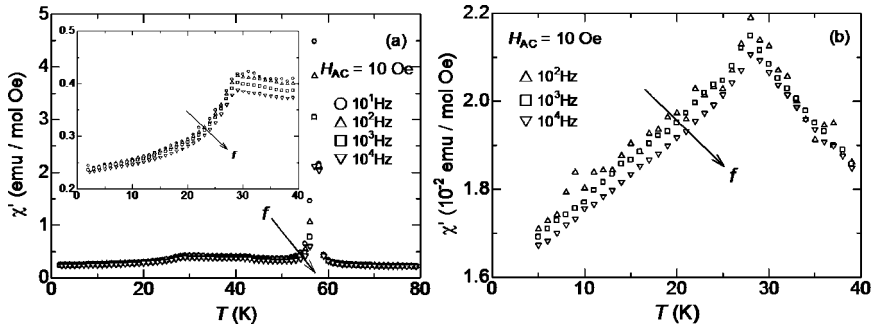

Figure 7. Real part $\chi'-T$ of the ac magnetic susceptibility for (a) red-$BiMn_7O_{12}$ and (b) ox-$BiMn_7O_{12}$. The magnitude of the ac field was 10 Oe and the frequency, f, varied from 10 to 10^4 Hz.

distortion (i.e., simultaneous increase in b and decrease in a, c, and β) is seen. Note that, as expected, the unit-cell volume V decreases with increasing z. This may be attributed to the increased concentration of the smaller Mn^{4+} ($3d\text{-}t_{2g}^3$) species at the expense of the larger Mn^{3+} ($3d\text{-}t_{2g}^3\text{-}e_g^1$) species with increasing oxygen-to-metal ratio. The apparent breakdown of the cooperative JT distortion of MnO_6 octahedra seen for the present $(BiMn_3)Mn_4O_{12\pm\delta}$ system with increasing concentration of cation vacancies is very parallel to the situation previously reported for the isostructural $[Ca(Mn_{1-x}Cu_x)_3]Mn_4O_{12}$ system[22] and also for a number of simple perovskite systems, e.g., $(La_{1-x}Ca_x)MnO_3$,[23] $La_{1-y}Mn_{1-y}O_3$,[24] and $La_{1-t}MnO_3$.[25]

Finally, we characterized the two essentially single-phase samples of $(BiMn_3)Mn_4O_{12\pm\delta}$ synthesized through route 1 (red-$BiMn_7O_{12}$) and route 2 (ox-$BiMn_7O_{12}$) for their basic electrical and magnetic properties. Resistivity measurements, carried out with a standard four-point-probe method under various magnetic fields, showed insulating/semiconducting behaviors (i.e., increasing resistivity values with decreasing temperature) with room-temperature resistivity values of approximately 10^4 Ω cm for both the phases, even at 7 T, hence indicating some carrier localization. Parallel results have been reported for $(NaMn_3)Mn_4O_{12}$[12] and $(CaMn_3)Mn_4O_{12}$.[20]

Magnetization measurements were performed with a superconducting quantum interference device magnetometer (SQUID; Quantum Design: MPMS-XL5) in both field-cooled (FC) and zero-field-cooled (ZFC) modes. Figure 5a shows the dependences of magnetization on temperature for red-$BiMn_7O_{12}$ and ox-$BiMn_7O_{12}$. For the former, two magnetic transitions are observed, at $T_1 \approx 28$ K and $T_2 \approx 59$ K, whereas the latter shows only the lower-temperature transition at ~27 K. Note that the isostructural $(LaMn_3)Mn_4O_{12}$ phase shows two antiferromagnetic transitions at 20 and 76 K, assigned to Mn^{3+}-ion spin orderings at the A″-site and the B-site, respectively.[26] In contrast to the case of $(LaMn_3)Mn_4O_{12}$, a ferromagnetic hysteresis was observed for our red-$BiMn_7O_{12}$ sample at temperatures below 59 K. The resultant spontaneous magnetization (~1 μ_B/formula unit with seven Mn^{3+} ions) is, however, relatively small and points, hence, toward some spin-canting or ferrimagnetic ordering.[14] A neutron diffraction study has been initiated to solve the detailed crystallographic and magnetic structures of red-$BiMn_7O_{12}$ and ox-$BiMn_7O_{12}$.

Below T_1, a large difference is observed between the ZFC and FC curves for both red-$BiMn_7O_{12}$ and ox-$BiMn_7O_{12}$ (see Figure 5a), indicating some frustrated state. The branching of the ZFC and FC magnetization curves was gradually suppressed with increasing external magnetic field (not shown here). As seen in Figure 5b, the dependence of magnetization on field at 5 K exhibits some hysteresis for both red-$BiMn_7O_{12}$ and ox-$BiMn_7O_{12}$, indicating some small ferromagnetic component. The inverse FC-susceptibility is shown in Figure 6 for ox-$BiMn_7O_{12}$ with respect to temperature at different magnetic fields. The phase transition temperature as defined at the onset of the plateau shifts toward the lower temperature side and becomes rapidly smeared out with increasing field such that the ox-$BiMn_7O_{12}$ phase may be magnetically frustrated.

In order to investigate the magnetic-frustration-like characteristics in detail, ac magnetic susceptibility measurements were carried out for both the red-$BiMn_7O_{12}$ and ox-$BiMn_7O_{12}$ samples using an ac magnetometer (Quantum Design, PPMS 6000) in the frequency range of $10-10^4$ Hz under an ac magnetic field of 10 Oe; see Figure 7. Figure 7b shows that for ox-$BiMn_7O_{12}$ the cusp temperature (due to the magnetic transition about 27 K) does not depend on frequency (f), whereas below the cusp, χ' is clearly dependent on f. This indicates that the magnetic transition observed for ox-$BiMn_7O_{12}$ may not be due to a spin-glass-like magnetic competition. Since a parallel feature is seen for red-$BiMn_7O_{12}$ below 28 K (see Figure 7a), we may conclude that the dc and ac susceptibility data for ox-$BiMn_7O_{12}$ are consistent if the state is of a frustrated magnetic state, just as for the case of red-$BiMn_7O_{12}$ below 28 K. In other words, the cation-deficient phase of ox-$BiMn_7O_{12}$ shows yet a frustrated AFM state below 27 K, as the case of red-$BiMn_7O_{12}$ at lower

(22) Sławiński, W.; Przeniosło, R.; Sosnowska, I.; Bieringer, M.; Margiolaki, I.; Fitch, A. N.; Suard, E. *J. Solid State Chem.* **2006**, *179*, 2443.
(23) Wollan, E. O.; Koehler, W. C. *Phys. Rev.* **1955**, *100*, 545.
(24) Okamoto, H.; Fjellvåg, H.; Yamauchi, H.; Karppinen, M. *Solid State Commun.* **2006**, *137*, 522.
(25) Hauback, B. C.; Fjellvåg, H.; Sakai, N. *J. Solid State Chem.* **1996**, *124*, 43.
(26) Prodi, A.; Allodi, G.; Gilioli, E.; Marezio, M.; Bolzoni, F.; Gauzzi, A.; Renzi, R. De. *Physica B* **2006**, *374–375*, 55.
(27) Karppinen, M.; Yamauchi, H. Oxygen engineering for functional oxide materials. In *International Book Series: Studies of High Temperature Superconductors*; Narlikar, A. V., Ed.; Nova Science Publishers: New York 2001; Vol. 37, pp 109−143. Karppinen, M.; Yamauchi, H. Chemical design of copper-oxide superconductors: Homologous series and oxygen engineering. In *Frontiers in Superconducting Materials*; Narlikar, A. V., Ed.; Springer Verlag: Berlin, 2005; pp 255−294.

temperatures. On the other hand, no transition corresponding to the higher temperature magnetic transition observed for red-$BiMn_7O_{12}$ appears for ox-$BiMn_7O_{12}$ (see Figures 5 and 7). This situation may be compared with that of the simple perovskite $La_{1-x}Mn_{1-y}O_3$ system,[24,25] where the appearance of ferromagnetic couplings strongly depends on the oxygen content/concentration of cation vacancies.

In conclusion, we synthesized samples with different degrees of oxygenation of the novel A-site-ordered manganese perovskite system $(BiMn_3)Mn_4O_{12\pm\delta}$, and showed that the monoclinic distortion seen for the least-oxygenated samples was gradually suppressed with increasing oxygen content (or with increasing concentration of cation vacancies) such that the most highly oxygenated samples possess a cubic perovskite structure. The less oxygenated monoclinic $(BiMn_3)Mn_4O_{12\pm\delta}$ phase showed two magnetic transitions, at 28 and 59 K, whereas the more highly oxygenated $(BiMn_3)Mn_4O_{12\pm\delta}$ phase of a cubic crystal structure was found to lack the higher-temperature transition. This suggests that monoclinic distortion (or a network of octahedral MnO_6 with cooperative JT distortion) assists the formation of a long-range magnetic ordering between the B-site Mn^{3+} ions. The present work has hence demonstrated an attractive but not-yet-utilized possibility to tailor the properties of the $(A'A''_3)B_4O_{12\pm\delta}$-type ordered perovskite oxides by means of oxygen-content control or of oxygen engineering.[27]

Acknowledgment. The present work was supported by Tekes (No. 1726/31/07) and Academy of Finland (Nos. 114517 and 116254).

CM803030X